Tuneable Time Delay in the Burst Release from Oxidation-Sensitive Polymersomes Made by PISA

Fabian H. Sobotta, Maren T. Kuchenbrod, Franka V. Gruschwitz, Grit Festag, Peter Bellstedt, Stephanie Hoeppener, and Johannes C. Brendel*

Abstract: Reactive polymersomes represent a versatile artificial cargo carrier system that can facilitate an immediate release in response to a specific stimulus. The herein presented oxidation-sensitive polymersomes feature a time-delayed release mechanism in an oxidative environment, which can be precisely adjusted by either tuning the membrane thickness or partial pre-oxidation. These polymeric vesicles are conveniently prepared by PISA allowing the straightforward and effective in situ encapsulation of cargo molecules, as shown for dyes and enzymes. Kinetic studies revealed a critical degree of oxidation causing the destabilization of the membrane, while no release of the cargo is observed beforehand. The encapsulation of glucose oxidase directly transforms these polymersomes into glucose-sensitive vesicles, as small molecules including sugars can passively penetrate their membrane. Considering the ease of preparation, these polymersomes represent a versatile platform for the confinement and burst release of cargo molecules after a precisely adjustable time span in the presence of specific triggers, such as H_2O_2 or glucose.

Introduction

Polymeric vesicles, or polymersomes, are bilayer nanostructures which are composed of an aqueous inner compartment enclosed by a polymer membrane. In the last years, several reports have pointed out their potential as drug delivery systems or nanoreactors, as hydrophilic cargos, such as nucleic acids[1] or enzymes,[2] can be internalized in the hydrophilic center or hydrophobic drugs are incorporated in the bilayer.[3] This compartmentalization can be used to protect and confine reactants or catalysts for defined periods of time with the aim to control the release kinetics.[4] By mimicking the properties of natural vesicles to respond to external stimuli, the accessibility of the cargo can be manipulated to enhance the diffusion into the exterior by changing the membrane permeability,[5] triggering a pore formation[6] or complete membrane disassembly.[7] In contrast to liposomes, polymer-based vesicles provide improved chemical diversity and allow for a facilitated introduction of stimuli-responsive groups in the vesicular structure.[8] Depending on the type of functionality, the polymersomes may respond to external stimuli, such as pH,[9] temperature[10] or redox potential.[11] Especially polymersomes which are sensitive to the presence of oxidants, such as reactive oxygen species (ROS), are of high interest, however, the number of reported systems remains limited.[12] ROS represents a class of highly oxidizing substances, including singlet oxygen, different peroxides, and superoxides. Their excessive production is related to inflammations caused by diseases like cancer or neurological disorders and represents a suitable trigger for the selective release of therapeutics.[13] Besides common motifs, such as boronic acid ester[14] and oxalates,[15] poly-(propylsulfide) (PPS)[16] represents one of the most frequently used materials for oxidation-responsive systems. Their oxidative response is based on a rapid switch from a hydrophobic to a strongly hydrophilic material due to the oxidation of the sulfide moieties to sulfoxides or sulfones. We have previously reported that *N*-acryloylthiomorpholine (NAT) responds in a similar way to oxidative stimuli, such as H_2O_2, while it is furthermore suitable to form nanostructures in situ via polymerization-induced self-assembly (PISA).[17] PISA represents a versatile technique for the simultaneous polymerization and self-assembly of block copolymers into nanostructures of different shapes.[18] In contrast to many other techniques, polymersomes can be formed at high concentrations, which facilitates high encapsulation efficiencies. Another benefit of PISA is the possibility to modify structural parameters by adjusting the initial conditions of the polymerization. For instance, changing the type and length of the hydrophilic block allows the modification of the vesicle diameter,[19] whereas the membrane thickness can be tuned by adjusting the molar mass of the hydrophobic block.[20] Therefore, aqueous PISA has been frequently used to build functional polymersomes including drug delivery vehicles or nanoreactors.[2a,21] However, stimuli-responsive polymersome

[*] F. H. Sobotta, M. T. Kuchenbrod, F. V. Gruschwitz, Dr. G. Festag,
Dr. P. Bellstedt, Dr. S. Hoeppener, Dr. J. C. Brendel
Laboratory of Organic and Macromolecular Chemistry (IOMC)
Friedrich Schiller University Jena
Humboldtstrasse 10, 07743 Jena (Germany)
E-mail: J. C. Brendel ()
E-mail: johannes.brendel@uni-jena.de

F. H. Sobotta, M. T. Kuchenbrod, F. V. Gruschwitz, Dr. G. Festag,
Dr. S. Hoeppener, Dr. J. C. Brendel
Jena Center for Soft Matter (JCSM)
Friedrich Schiller University Jena
Philosophenweg 7, 07743 Jena (Germany)

formations by PISA remain scarce and respective studies mainly focus on pH-responsive systems,[21a,22] while to the best of our knowledge only a single oxidation-sensitive system has been reported.[23]

Recently, we were able to demonstrate that various nanostructures including polymersomes are accessible within the PISA of NAT,[24] which prompted us to investigate their potential for in situ encapsulation and selective release of cargo molecules in an oxidative environment. Dynamic light scattering (DLS) and NMR measurements were applied to evaluate the time-dependent degradation and oxidation, respectively, of polymersomes featuring different membrane thicknesses. In addition, the integrity of the vesicular membrane at different time points was analyzed by cryo-transmission electron microscopy (cryo-TEM). The encapsulation and time-dependent release were tested using the model fluorophore calcein. In addition, we encapsulated the functional enzyme glucose oxidase (GOx) for studying the membrane permeability, as it forms H_2O_2 in presence of glucose.

Results and Discussion

Based on our previous in-depth study on the morphological evolution of structures during the PISA process,[24] vesicular structures with different hydrophobic block lengths can be prepared by aqueous RAFT dispersion polymerization of NAT in the presence of $PNAM_{25}$ as macro-chain transfer agents (mCTA). The mCTA can conveniently be accessed by aqueous RAFT polymerization without the need for any further purification as full conversions of the monomer are reached. Setting appropriate conditions, the $PNAM_{25}$ is directly chain extended with different NAT/mCTA feed ratios (25, **V1**; 50, **V2** and 70, **V3**) to obtain unilamellar vesicles in aqueous dispersions. Interestingly, the obtained vesicles are of comparable sizes (Table S1), while the membrane thickness (D_M) successively increases with increasing degree of polymerization (DP) of PNAT from a mean D_M of ≈ 13 nm for a DP of 25 to ≈ 17 nm for DP 50 and ≈ 19 nm for a DP of 70 (determined by statistical analysis of cryo-TEM images, Figure 1 A–C, S2, S3).
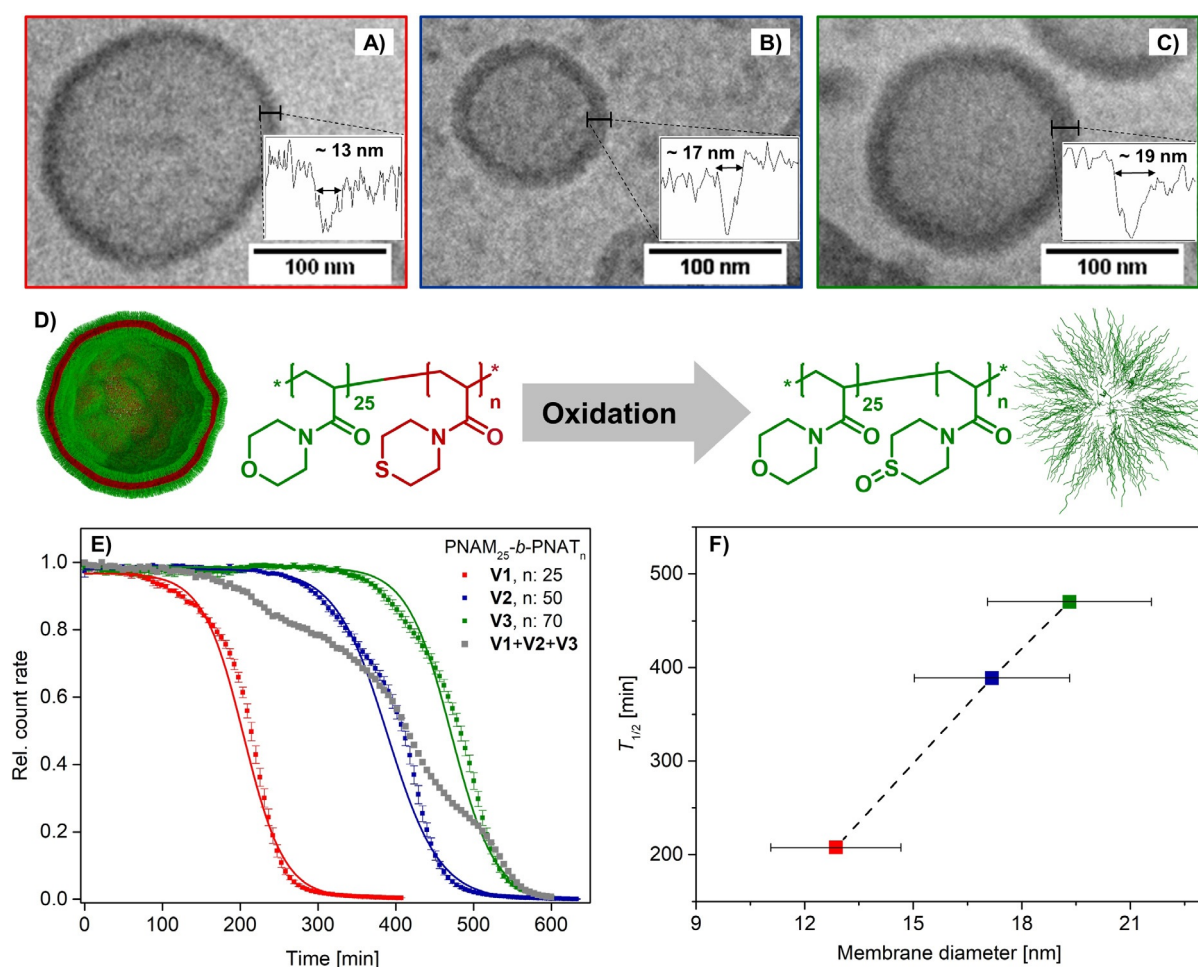

Figure 1. Influence of the DP of the hydrophobic block and the membrane thickness on the degradation behavior. The membrane diameter was determined from cryo-TEM images of the different vesicle samples: A) **V1** based on $PNAM_{25}$-*b*-$PNAT_{25}$. B) **V2** based on $PNAM_{25}$-*b*-$PNAT_{50}$. C) **V3** based on $PNAM_{25}$-*b*-$PNAT_{70}$. D) Vesicle degradation via oxidation of the core-forming block. E) Time-dependent decrease in count rate determined by DLS of separate samples **V1-3** (three individual replicates) and an equal mixture of **V1**+**V2**+**V3** (100 mM H_2O_2, 1 mg mL^{-1}, 37°C, PBS pH 7). F) Correlation of vesicular $T_{1/2}$, determined by fitting of the DLS degradation curves with the membrane diameter determined by graphical analysis of >100 cryo-TEM images.

We subsequently investigated the oxidative-triggered degradation of these vesicles in 100 mM H_2O_2 and analyzed the degradation process by time-dependent DLS measurements (Figure 1 E). In all cases, the count rate decreased only after a specific retardation time, following a rapid decay until the values became comparable to solutions containing free polymer chains. The sigmoidal shape of the decay indicates the predominance of a bulk mechanism rather than an interfacial reaction, which was already reported for nanostructures based on PPS.[25] Interestingly, the hydrodynamic diameter (D_H) of all structures remains constant until the degradation process starts. Close to this point, it increases slightly before a rapid decay is observed coinciding with the decrease in count rate (Figure S5B). Apparently, the polymersomes seem to remain intact for hours of incubation until they suddenly fall apart at a certain critical time point. The individual degradation points can even be observed in mixtures of the three different vesicles **V1-3** (Figure 1 E, gray squares), which displayed distinct steps at the characteristic degradation times for the individual vesicles. The individual degradation profiles could be approximated by a Boltzmann function to determine the respective $T_{1/2}$ of each vesicle in H_2O_2. The comparison of the $T_{1/2}$ to the D_M, as determined by cryo-TEM, revealed a linear correlation, which suggests that the degradation time is mainly dependent on the thickness of the vesicular membrane. Thus, the variation of the molar mass of the PNAT block and hence the membrane thickness provides the possibility to modulate the point of degradation of these polymersomes.

In order to further investigate the degradation mechanism, we performed a kinetic study on a larger batch of vesicles **V3** in 100 mM H_2O_2 by taking samples at certain reaction times (100 mL, 1 mg mL^{-1}, 37°C, PBS pH 7.4). The samples were instantly diluted in an excess of aqueous $Na_2S_2O_3$ solution (0.2 M) and cooled down to quench the oxidation reaction. The characteristic self-accelerating decay (count rate and D_H) after ≈ 7 h for **V3** (Figure 1 E) observed during the previous time-dependent DLS measurements

could be reconstructed, which suggests the successful quenching of the oxidation reaction (Figure 2). For selected samples close to the onset of degradation, cryo-TEM images were acquired (Figure 2 I–IV). The micrographs revealed that after an incubation time of 350 min, the vesicular structure remained still intact (Figure 2 I, S4A). Even after 420 min, when the count rate starts to decay, the vesicles still seem to be stable without obvious signs of degradation (Figure 2 II, S4B). One hour later at 484 min, the count rate drops significantly ($\approx 40\%$) and the D_H increases. The corresponding cryo-TEM revealed almost exclusively vesicles with a ruptured or perforated membrane, respectively, and a few ones already start to unfold (Figure 2 III, S4C). Just 30 min later at 514 min, the vesicular structures are completely fallen apart and only membrane fragments are observed (Figure 2 IV, S4D). In order to correlate the structural information to the PNAT oxidation kinetics, the degree of oxidation of the quenched samples was determined by NMR. First, the samples were purified from the residual $Na_2S_2O_3$ and PBS by dialysis. After lyophilization NMR spectra were collected in a 4:1 volume mixture of [D_8]THF:D_2O, which was found to be the best solvent for dissolution of both the unoxidized and oxidized polymer while reducing the interferences by the overlap of signals. Due to the strong broadening of the proton signals, rapid $^1H,^{13}C$-heteronuclear single quantum correlation (ASAP-HSQC) experiments were performed to clearly separate oxidized from non-oxidized species.[26] For calculating the degree of oxidation, the shifts of the CH_2 proton signals in α-position to the sulfur atom (1.7/26.1 ppm to 2.7/32.6 ppm, 3.1/36.3 ppm, 3.4/32.6 ppm) were compared (Figure S6–S8). The degree of oxidation revealed that the oxidation of PNAT followed a continuous exponential increase up to a degree of oxidation of $\approx 65\%$ during the incubation time (Figure 2, S9). Only the final two time points, at 554 and 600 min, reveal a slight decrease again (marked with *), which is related to the limited solubility of the sulfoxide polymer in the applied THF mixture that was required to maintain comparability. The exponential increase
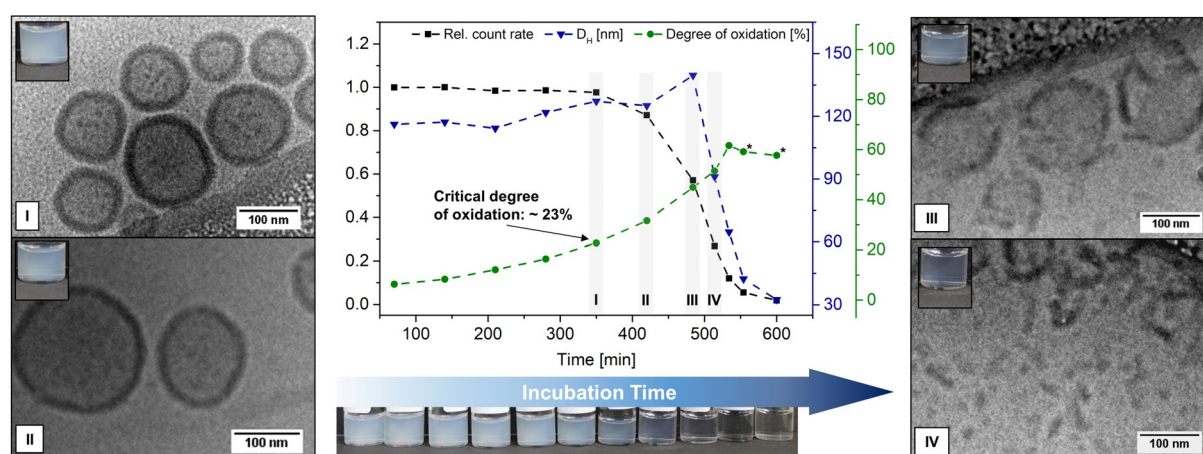

Figure 2. Kinetic study of the oxidation-triggered disintegration of PNAM$_{25}$-*b*-PNAT$_{70}$-based vesicles **V3** (100 mM H_2O_2, 1 mg mL^{-1} PBS, 37°C, pH 7). The correlation of vesicle rupture was analyzed by DLS and the degree of oxidation was determined by ASAP-HSQC NMR of quenched samples (8 mL, 0.2 M $Na_2S_2O_3$, 4/-20°C), while cryo-TEM images were recorded of quenched samples after 350 (I), 420 (II), 484 (III), and 514 min (IV). * Samples not completely dissolved.
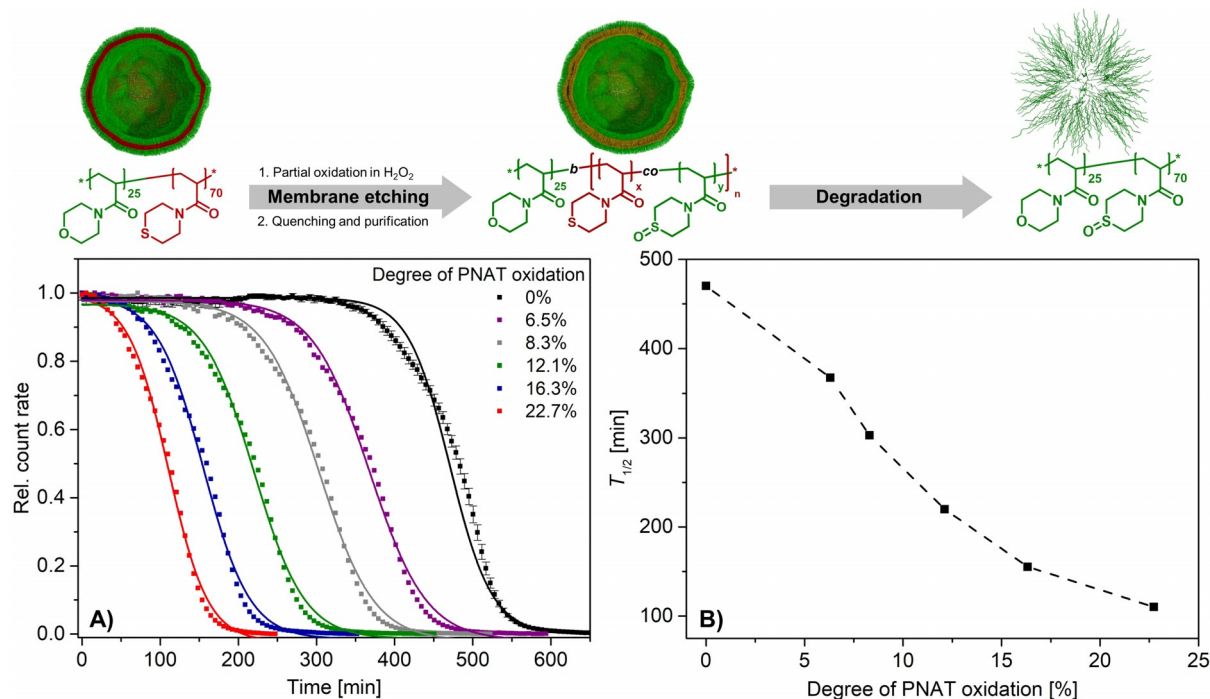
Figure 3. Adjustment of vesicular half-life time $T_{1/2}$ by membrane etching. A) Time-dependent decrease in count rate determined by DLS of partially oxidized vesicles **V3** (100 mM H_2O_2, 1 mg mL^{-1} PBS, 37°C, pH 7). B) Correlation of $T_{1/2}$ with the degree of oxidation of the PNAT block as determined by NMR.

during the polymer oxidation is typical for a self-accelerating reaction and reflects the increased accessibility of the H_2O_2 to the thioethers in the hydrophobic domain due to the change in polarity from polysulfide to polysulfoxide.[27] On the other hand, the lack of an initial retardation period indicates that the oxidation process is not impeded by the hydrophobic membrane and follows a similar bulk mechanism as observed for the degradation profile, which implies a sufficient permeability of the PNAT membrane towards H_2O_2. Correlating the NMR data with the DLS and cryo-TEM data, a critical degree of oxidation of $\approx 23\%$ was determined at which the PNAT membrane was partially oxidized, but still retained its mechanical stability (Figure 2I). Based on this finding, we tested whether partial membrane oxidation could be used to further tune the degradation time, similar to the influence of the variation of the membrane diameter. Therefore, the membrane of the PNAM$_{25}$-*b*-PNAT$_{70}$-based vesicles **V3** was partially oxidized or "etched" by oxidation in H_2O_2 solution and quenching at defined time points predetermined by the previous kinetic study. Comparison of the scattering profiles of the untreated and the partially oxidized vesicles **V3** proved the integrity of the vesicular structure even after long-term storage up to 6 months (Figure S10). After purification by dialysis, the complete degradation of the "etched" vesicles was monitored via DLS (Figure 3A, S5C). The count rates followed a similar sigmoidal decay as observed for untreated samples, however, the degradation time (represented by $T_{1/2}$) shifted in correlation with the initial degree of oxidation of the sample (Figure 3B). The results demonstrate that even though the membrane integrity was preserved at low degrees of oxidation, the sensitivity of the "etched" vesicles towards

oxidants is strongly increased and can be utilized to tailor the vesicular lifetime via pre-oxidation and quenching treatment.

As a next step, we investigated if the vesicles were also able to encapsulate and release a cargo at specific time points. Therefore, calcein was chosen as a hydrophilic model dye, which is known for its self-quenching of fluorescence when encapsulated at high concentrations in the vesicular lumen.[28] Upon release and dilution, a characteristic increase in the fluorescence intensity is observed. Calcein was conveniently encapsulated by adding a 1 mM solution to the above-described RAFT dispersion polymerization of NAT. It is noteworthy that higher calcein concentrations of 10 and 100 mM interfered with the RAFT process and impeded the polymerization. The polymersomes were separated from free calcein by preparative size-exclusion chromatography (SEC) and subsequent dialysis. The preparation of all three calcein-containing vesicles (**V1-3-C**) resulted in similar molar masses and dispersities, while slightly different D_H values were obtained, which are nevertheless in a similar range (Table S1, Figure S11A,B). The encapsulation efficiencies (EE) were determined by UV/Vis spectroscopy of lyophilized samples after vesicle dissolution (Table S1, Figure S13D). The excellent stability of these vesicles and capability to retain small molecules is further exemplified by asymmetric flow-field flow fractionation (AF4) measurements, where the calcein remains within the vesicles **V3-C** even after storage for > 1 year (Figure S12A,B). The localization of the calcein inside the aqueous lumen was indicated by comparing the fluorescence emission spectra of the calcein-loaded vesicles **V1-3-C** with free calcein in aqueous buffer and organic solvent (Figure S13E).
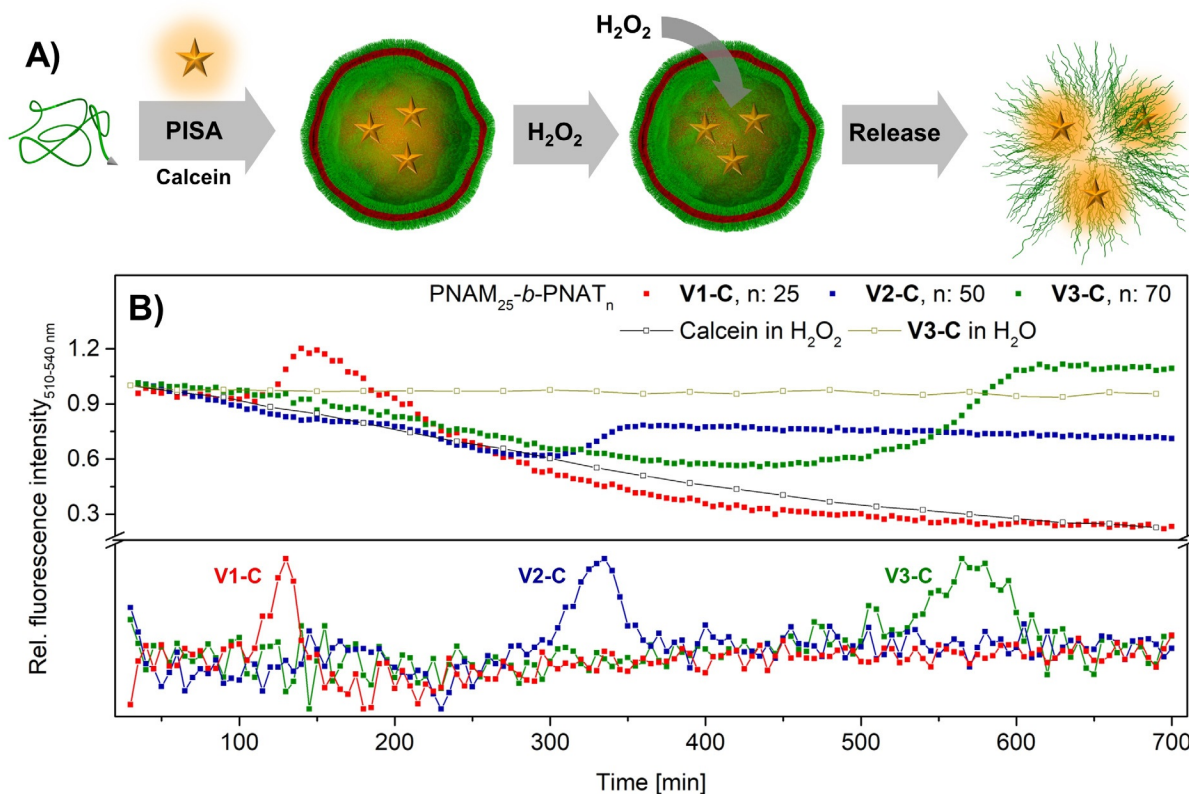
Figure 4. A) Schematic representation of the loading and oxidation-triggered release of calcein. B) Time-dependent fluorescence intensity of calcein-loaded vesicles **V1-3-C** incubated in 100 mM H_2O_2 (1.75 mg mL^{-1}, 37°C, PBS pH 7). **V3-C** in H_2O and calcein in 100 mM H_2O_2 acted as controls. Release events are indicated by the maxima of the 1st derivative of fluorescence intensity with time.

The release kinetics were investigated by incubating the calcein-loaded vesicles (**V1-3-C**) in 100 mM H_2O_2 in a cuvette and monitoring the calcein fluorescence intensity (Ex.: 495 nm, Em.: 510–540 nm; Figure 4B) over time. As H_2O_2 causes an oxidation-induced fluorescence quenching, free calcein was investigated under similar conditions as a reference.[29] In the case of the calcein-loaded vesicles (**V1-3-C**) in H_2O_2 a comparable continuous decrease in fluorescence intensity was observed at early stages. This continuous quenching of the encapsulated calcein, similar to free calcein, corroborates the above-mentioned free diffusion of H_2O_2 across the vesicular membrane. After a specific time for each tested sample, the release of calcein could be detected by a distinct increase in fluorescence intensity (Figure 4B). Similar to the $T_{1/2}$ values described above, the release shifts to later time points for larger PNAT blocks and correlates well with the onsets of membrane degradation of the unloaded vesicles **V1-2**. We assume that the delay in **V3** is related to a decrease of the H_2O_2 concentration in presence of the dye, but it nevertheless shows a similar release pattern. In the case of the vesicles with the longer PNAT-blocks **V2-3-C**, the quenching of the calcein fluorescence was slowed down after the release, which might be a result of a decreased H_2O_2 concentration, due to the oxidation of the polymeric thioether groups. Overall, these results prove that the membrane of the vesicles remains intact and impermeable for larger molecules such as calcein even at an increased degree of oxidation, as no

leakage of the dye is observed prior to the disintegration point. This retarded release is highly desirable in drug delivery applications to prevent premature drug leakage while prolonging the circulation time to achieve high local concentrations.[30] Encouraged by these results and inspired by previous works on polymersomes utilized as nanoreactors,[31] we tested the encapsulation of functional and active enzymes. Glucose oxidase (GOx) appeared particularly attractive for encapsulation in this proof-of-concept study, as it catalyzes the formation of gluconic acid and H_2O_2 from glucose. A successful encapsulation would therefore render the polymersomes responsive to glucose, but only if the latter is able to cross the polymer membrane. In contrast to the calcein encapsulation, the PISA process had to be slightly adapted to prevent denaturation of the enzyme. As a consequence, the temperature for the RAFT polymerization was reduced to 40°C, which required an increase of initiator concentration and an extension of the polymerization time to 20 hours. Furthermore, the 1,4-dioxane content was increased to 33 vol% to ensure sufficient chain mobility and vesicle formation. After the reaction, the excess of the free enzyme was removed via preparative SEC in buffer solution. Polymersomes of comparable sizes to the unloaded sample **V3** were obtained as confirmed by DLS, cryo-TEM, and AF4 measurements (Figure S11C,D, S12C-F, Table S1). SEC measurements of the GOx-loaded vesicles **V3-G** in aqueous buffer proved the successful purification and removal of any
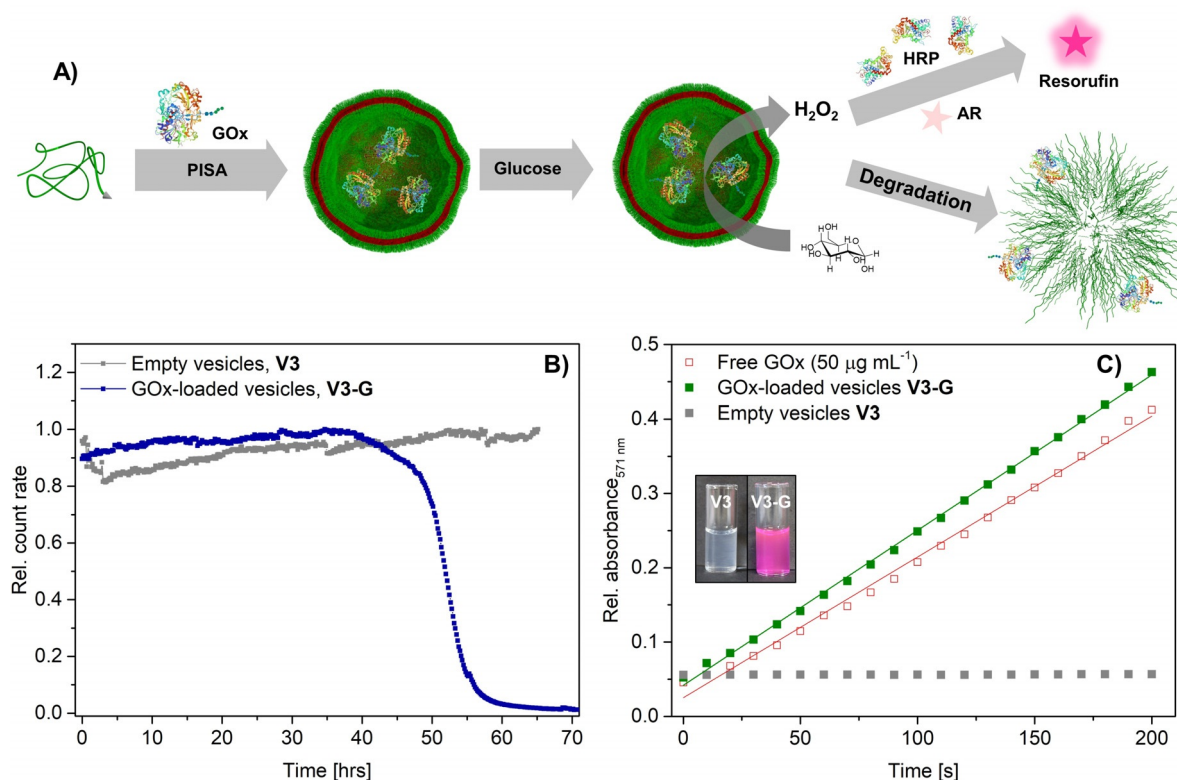
Figure 5. Loading and glucose-triggered membrane degradation of GOx-loaded vesicles. A) Schematic representation of the loading, cascade reaction, and degradation. B) Membrane destabilization of GOx-loaded vesicles **V3-G** monitored via time-dependent DLS measurements. **V3-G** and **V3** were incubated in 100 mM glucose solution (0.5 mg mL^{-1} in citrate-phosphate buffer, 37 °C, pH 7). C) Enzymatic activity of GOx-loaded vesicles **V3-G** determined by conversion of amplex red to pink-colored resorufin in comparison to free GOx (50 μg mL^{-1}).

remaining free GOx (Figure S1C,D). Since the membrane thickness was determined to be comparable to the unloaded vesicles (Table S1, Figure S3D), the GOx was expected to be internalized into the vesicular lumen similarly to previously reported systems.[32] However, adsorption of the GOx to the inner vesicular membrane cannot be fully excluded. In a first approach, the activity of the encapsulated GOx was assessed by performing a cascade reaction with horseradish peroxidase (HRP) and amplex red (AR) as a fluorescent probe (Figure 5 A, S13A). The assay enables the detection of even small amounts of H$_2$O$_2$ released in the reaction of GOx and glucose, as the HRP catalyzes the conversion of the non-colored AR to the pink-colored resorufin. In our case, however, the glucose must first diffuse through the vesicular membrane to reach the encapsulated GOx and start the reaction cascade.

The reaction was followed by monitoring the absorbance at 571 nm directly after glucose addition (Figure 5 C). The solution of **V3-G** rapidly turned pink and showed a steady increase in absorbance, indicating a high GOx activity and steady penetration of glucose through the membrane. As a control, empty vesicles **V3** showed no activity under the same conditions. Comparing the reaction rate of **V3-G** with samples of defined GOx concentrations, the amount of encapsulated, active GOx could be determined resulting in an EE of 34 % (see SI for calculation, Figure 5 C, S13B,C). The high EE reflects once more the potential of PISA for the effective encapsulation of enzymes.[2b,10c] It should be noted

that the real EE might be even higher, since the reaction might be retarded compared to the free enzyme, due to the diffusive barrier formed by the membrane. Apart from that, the high activity observed for the encapsulated GOx indicates an inherent size-selective permeability of the PNAT membrane towards small hydrophilic molecules, such as glucose or H$_2$O$_2$, while slightly larger molecules, such as calcein, and the macromolecule GOx, were retained in the vesicular lumen. As PNAT features a high glass transition temperature, this intrinsic permeability of the membrane likely originates from increased hydration of the PNAT domain,[33] similar to previous observations for PHPMA-based systems.[2b,5a,34] Subsequent to these permeability studies, we assessed whether the H$_2$O$_2$ generation of the encapsulated GOx is sufficient to induce the oxidation of the thioether groups and finally destabilize the vesicular membrane. Therefore, the GOx-loaded vesicles **V3-G** and empty vesicles **V3** were incubated in a glucose solution, and the membrane stability was monitored in time-dependent DLS measurements (Figure 5 B, S5D). A similar self-accelerating decay in count rate, as found for the degradation in H$_2$O$_2$, was observed for **V3-G** after ≈ 48 hours of incubation. The control sample **V3** showed no degradation within the measurement time. The results prove that the GOx-loaded vesicles not only maintain a high enzyme activity but are additionally capable of inducing a self-degradation mechanism in the presence of glucose as a trigger.

Conclusion

In summary, we have developed oxidation-sensitive polymersomes featuring a distinct disintegration with a sharp onset after a specific exposure time to an oxidative environment. The thioether-based PNAT can be conveniently prepared by PISA in an aqueous RAFT dispersion polymerization. A detailed kinetic study of the degradation mechanism revealed that the polymersomes disintegrate rapidly at a critical degree of oxidation. A bulk degradation mechanism was observed which implies a high diffusion rate of H_2O_2 into the PNAT membrane. Varying the DP of the hydrophobic PNAT block, the membrane thickness can be adjusted, which directly correlates with different disintegration times. An additional strategy to modulate the lifetime of the polymersomes relies on the observed high stability of the membrane before reaching a critical degree of oxidation. In this approach, the PNAT membrane can be partially oxidized or "etched" and subsequently quenched. In a first proof of concept, calcein was successfully encapsulated as a model dye inside these vesicles. A release was only observed after reaching the critical degree of oxidation causing the full disintegration of the membrane. The presented polymersomes, therefore, represent ideal delivery vehicles for time-controlled release, which can be conveniently adjusted by the strategies described above. In addition, we demonstrate the encapsulation of GOx as an active enzyme. The retained activity of the enzyme not only demonstrates the high permeability of the PNAT membrane towards small hydrophilic molecules but also transforms the polymersomes into glucose-responsive, self-degrading nanoreactors by the conversion of glucose to H_2O_2. Overall, the convenient preparation pathway and the high EE render these polymersomes a versatile platform for controlled delivery which can be adapted to a range of different cargo molecules and conditions. In further perspective, the presented system can be adapted to modulate the accessibility of reactants during multicomponent reactions or release encapsulated therapeutics in areas of high glucose concentrations and oxidative stress, such as diabetic or tumor tissue,[35] in a time- and concentration-controlled manner.

Acknowledgements

Conflict of Interest

The authors declare no conflict of interest.

[1] a) S. Iqbal, M. Blenner, A. Alexander-Bryant, J. Larsen, *Biomacromolecules* **2020**, *21*, 1327–1350; b) H. Lomas, I. Canton, S. MacNeil, J. Du, S. P. Armes, A. J. Ryan, A. L. Lewis, G. Battaglia, *Adv. Mater.* **2007**, *19*, 4238–4243.

[2] a) L. D. Blackman, S. Varlas, M. C. Arno, Z. H. Houston, N. L. Fletcher, K. J. Thurecht, M. Hasan, M. I. Gibson, R. K. O'Reilly, *ACS Cent. Sci.* **2018**, *4*, 718–723; b) L. D. Blackman, S. Varlas, M. C. Arno, A. Fayter, M. I. Gibson, R. K. O'Reilly, *ACS Macro Lett.* **2017**, *6*, 1263–1267; c) C. Z. Bueno, A. C. Apolinário, A. Duro-Castano, A. Poma, A. Pessoa, C. O. Rangel-Yagui, G. Battaglia, *ACS Macro Lett.* **2020**, *9*, 1471–1477.

[3] S. Matoori, J.-C. Leroux, *Mater. Horiz.* **2020**, *7*, 1297–1309.

[4] D. E. Discher, A. Eisenberg, *Science* **2002**, *297*, 967.

[5] a) S. Varlas, J. C. Foster, P. G. Georgiou, R. Keogh, J. T. Husband, D. S. Williams, R. K. O'Reilly, *Nanoscale* **2019**, *11*, 12643–12654; b) G. Cheng, J. Pérez-Mercader, *Chem. Mater.* **2019**, *31*, 5691–5698; c) H. Che, S. Cao, J. C. M. van Hest, *J. Am. Chem. Soc.* **2018**, *140*, 5356–5359.

[6] a) K. T. Kim, J. J. L. M. Cornelissen, R. J. M. Nolte, J. C. M. van Hest, *Adv. Mater.* **2009**, *21*, 2787–2791; b) P. Shi, Y. Qu, C. Liu, H. Khan, P. Sun, W. Zhang, *ACS Macro Lett.* **2016**, *5*, 88–93; c) W.-J. Zhang, C.-Y. Hong, C.-Y. Pan, *ACS Appl. Mater. Interfaces* **2017**, *9*, 15086–15095.

[7] a) X.-R. You, X.-J. Ju, F. He, Y. Wang, Z. Liu, W. Wang, R. Xie, L.-Y. Chu, *ACS Appl. Mater. Interfaces* **2017**, *9*, 19258–19268; b) G. Liu, X. Wang, J. Hu, G. Zhang, S. Liu, *J. Am. Chem. Soc.* **2014**, *136*, 7492–7497.

[8] J. Lefley, C. Waldron, C. R. Becer, *Polym. Chem.* **2020**, *11*, 7124–7136.

[9] a) F. Ahmed, D. E. Discher, *J. Controlled Release* **2004**, *96*, 37–53; b) K. Dan, S. Ghosh, *Angew. Chem. Int. Ed.* **2013**, *52*, 7300–7305; *Angew. Chem.* **2013**, *125*, 7441–7446.

[10] a) Y. Li, B. S. Lokitz, C. L. McCormick, *Angew. Chem. Int. Ed.* **2006**, *45*, 5792–5795; *Angew. Chem.* **2006**, *118*, 5924–5927; b) A. O. Moughton, R. K. O'Reilly, *Chem. Commun.* **2010**, *46*, 1091–1093; c) J. He, J. Cao, Y. Chen, L. Zhang, J. Tan, *ACS Macro Lett.* **2020**, *9*, 533–539.

[11] a) A. Napoli, M. Valentini, N. Tirelli, M. Muller, J. A. Hubbell, *Nat. Mater.* **2004**, *3*, 183–189; b) K. N. Power-Billard, R. J. Spontak, I. Manners, *Angew. Chem. Int. Ed.* **2004**, *43*, 1260–1264; *Angew. Chem.* **2004**, *116*, 1280–1284.

[12] a) Y. Deng, H. Chen, X. Tao, F. Cao, S. Trépout, J. Ling, M.-H. Li, *Biomacromolecules* **2019**, *20*, 3435–3444; b) E. Jäger, V. Sincari, L. J. C. Albuquerque, A. Jäger, J. Humajova, J. Kucka, J. Pankrac, P. Paral, T. Heizer, O. Janouskova, R. Konefał, E. Pavlova, O. Sedlacek, F. C. Giacomelli, P. Pouckova, L. Sefc, P. Stepanek, M. Hruby, *Biomacromolecules* **2020**, *21*, 1437–1449; c) G. Saravanakumar, H. Park, J. Kim, D. Park, J. Lim, J. Lee, W. J. Kim, *J. Controlled Release* **2020**, *327*, 627–640.

[13] a) M. Valko, D. Leibfritz, J. Moncol, M. T. Cronin, M. Mazur, J. Telser, *Int. J. Biochem. Cell Biol.* **2007**, *39*, 44–84; b) K. Apel, H. Hirt, *Annu. Rev. Plant Biol.* **2004**, *55*, 373–399.

[14] J. Kim, K. T. Kim, *ACS Appl. Mater. Interfaces* **2020**, *12*, 23502–23513.

[15] D. Lee, S. Bae, D. Hong, H. Lim, J. H. Yoon, O. Hwang, S. Park, Q. Ke, G. Khang, P. M. Kang, *Sci. Rep.* **2013**, *3*, 2233.

[16] a) S. Bobbala, S. D. Allen, S. Yi, M. Vincent, M. Frey, N. B. Karabin, E. A. Scott, *Nanoscale* **2020**, *12*, 5332–5340; b) K. M. Poole, C. E. Nelson, R. V. Joshi, J. R. Martin, M. K. Gupta, S. C.

Haws, T. E. Kavanaugh, M. C. Skala, C. L. Duvall, *Biomaterials* **2015**, *41*, 166–175; c) A. E. Vasdekis, E. A. Scott, C. P. O'Neil, D. Psaltis, J. A. Hubbell, *ACS Nano* **2012**, *6*, 7850–7857.

[17] F. H. Sobotta, F. Hausig, D. O. Harz, S. Hoeppener, U. S. Schubert, J. C. Brendel, *Polym. Chem.* **2018**, *9*, 1593–1602.

[18] a) S. Y. Khor, J. F. Quinn, M. R. Whittaker, N. P. Truong, T. P. Davis, *Macromol. Rapid Commun.* **2019**, *40*, 1800438; b) W. J. Zhang, C. Y. Hong, C. Y. Pan, *Macromol. Rapid Commun.* **2019**, *40*, 1800279.

[19] a) C. Gonzato, M. Semsarilar, E. R. Jones, F. Li, G. J. Krooshof, P. Wyman, O. O. Mykhaylyk, R. Tuinier, S. P. Armes, *J. Am. Chem. Soc.* **2014**, *136*, 11100–11106; b) J. Lesage de la Haye, X. Zhang, I. Chaduc, F. Brunel, M. Lansalot, F. D'Agosto, *Angew. Chem. Int. Ed.* **2016**, *55*, 3739–3743; *Angew. Chem.* **2016**, *128*, 3803–3807; c) M. Huo, Z. Xu, M. Zeng, P. Chen, L. Liu, L.-T. Yan, Y. Wei, J. Yuan, *Macromolecules* **2017**, *50*, 9750–9759.

[20] a) S. Pearce, J. Perez-Mercader, *Polym. Chem.* **2021**, *12*, 29–49; b) N. J. Warren, O. O. Mykhaylyk, A. J. Ryan, M. Williams, T. Doussineau, P. Dugourd, R. Antoine, G. Portale, S. P. Armes, *J. Am. Chem. Soc.* **2015**, *137*, 1929–1937.

[21] a) X.-F. Xu, C.-Y. Pan, W.-J. Zhang, C.-Y. Hong, *Macromolecules* **2019**, *52*, 1965–1975; b) C. J. Mable, R. R. Gibson, S. Prevost, B. E. McKenzie, O. O. Mykhaylyk, S. P. Armes, *J. Am. Chem. Soc.* **2015**, *137*, 16098–16108; c) J. Tan, H. Sun, M. Yu, B. S. Sumerlin, L. Zhang, *ACS Macro Lett.* **2015**, *4*, 1249–1253.

[22] a) M. Chen, J.-W. Li, W.-J. Zhang, C.-Y. Hong, C.-Y. Pan, *Macromolecules* **2019**, *52*, 1140–1149; b) C. J. Mable, I. Canton, O. O. Mykhaylyk, B. Ustbas Gul, P. Chambon, E. Themistou, S. P. Armes, *Chem. Sci.* **2019**, *10*, 4811–4821.

[23] S. Xu, G. Ng, J. Xu, R. P. Kuchel, J. Yeow, C. Boyer, *ACS Macro Lett.* **2017**, *6*, 1237–1244.

[24] F. H. Sobotta, M. Kuchenbrod, S. Hoeppener, J. C. Brendel, *Nanoscale* **2020**, *12*, 20171–20176.

[25] V. Khutoryanskiy Vitaliy, N. Tirelli, *Pure Appl. Chem.* **2008**, *80*, 1703.

[26] D. Schulze-Sünninghausen, J. Becker, B. Luy, *J. Am. Chem. Soc.* **2014**, *136*, 1242–1245.

[27] R. d'Arcy, A. Siani, E. Lallana, N. Tirelli, *Macromolecules* **2015**, *48*, 8108–8120.

[28] S. Cerritelli, D. Velluto, J. A. Hubbell, *Biomacromolecules* **2007**, *8*, 1966–1972.

[29] J.-M. Liu, Z.-b. Liu, Q. Huang, X. Lin, *Anal. Methods* **2014**, *6*, 8779–8784.

[30] a) T. Guo, T. Meng, G. Yang, Y. Wang, R. Su, S. Zhou, *Nano Lett.* **2019**, *19*, 6065–6071; b) M. A. Yassin, D. Appelhans, R. Wiedemuth, P. Formanek, S. Boye, A. Lederer, A. Temme, B. Voit, *Small* **2015**, *11*, 1580–1591.

[31] a) L. D. Blackman, Z. Y. Oo, Y. Qu, P. A. Gunatillake, P. Cass, K. E. S. Locock, *ACS Appl. Mater. Interfaces* **2020**, *12*, 11353–11362; b) S. F. M. van Dongen, M. Nallani, J. J. L. M. Cornelissen, R. J. M. Nolte, J. C. M. van Hest, *Chem. Eur. J.* **2009**, *15*, 1107–1114; c) J. Gaitzsch, X. Huang, B. Voit, *Chem. Rev.* **2016**, *116*, 1053–1093; d) H. Che, J. C. M. Van Hest, *ChemNanoMat* **2019**, *5*, 1092–1109.

[32] a) D. M. Vriezema, P. M. L. Garcia, N. Sancho Oltra, N. S. Hatzakis, S. M. Kuiper, R. J. M. Nolte, A. E. Rowan, J. C. M. van Hest, *Angew. Chem. Int. Ed.* **2007**, *46*, 7378–7382; *Angew. Chem.* **2007**, *119*, 7522–7526; b) S. M. Kuiper, M. Nallani, D. M. Vriezema, J. J. L. M. Cornelissen, J. C. M. van Hest, R. J. M. Nolte, A. E. Rowan, *Org. Biomol. Chem.* **2008**, *6*, 4315–4318.

[33] a) R. Takahashi, S. Miwa, F. H. Sobotta, J. H. Lee, S. Fujii, N. Ohta, J. C. Brendel, K. Sakurai, *Polym. Chem.* **2020**, *11*, 1514–1524; b) F. H. Sobotta, M. T. Kuchenbrod, C. Grune, D. Fischer, S. Hoeppener, J. C. Brendel, *Polym. Chem.* **2021**, *12*, 1668–1680.

[34] A. J. Miller, A. K. Pearce, J. C. Foster, R. K. O'Reilly, *ACS Cent. Sci.* **2021**, *7*, 30–38.

[35] a) J. Yu, C. Qian, Y. Zhang, Z. Cui, Y. Zhu, Q. Shen, F. S. Ligler, J. B. Buse, Z. Gu, *Nano Lett.* **2017**, *17*, 733–739; b) L. Zhao, L. Wang, Y. Zhang, S. Xiao, F. Bi, J. Zhao, G. Gai, J. Ding, *Polymers* **2017**, *9*, 255; c) W. Ke, J. Li, F. Mohammed, Y. Wang, K. Tou, X. Liu, P. Wen, H. Kinoh, Y. Anraku, H. Chen, K. Kataoka, Z. Ge, *ACS Nano* **2019**, *13*, 2357–2369.